ARTICLES

Solvent Relaxation Study of pH-Dependent Hydration of Poly(oxyethylene) Shells in Polystyrene-*block*-poly(2-vinylpyridine)-*block*-poly(oxyethylene) Micelles in Aqueous Solutions

Jana Humpolíčková,[†,‡] Miroslav Štěpánek,[†] Karel Procházka,*[,†] and Martin Hof[‡]

Department of Physical and Macromolecular Chemistry and Laboratory of Specialty Polymers, School of Science, Charles University in Prague, Albertov 2030, 128 40 Prague 2, Czech Republic, and Jaroslav Heyrovský Institute of Physical Chemistry of the Academy of Sciences of the Czech Republic, Dolejškova 3, 182 23 Prague 8, Czech Republic

Received: June 21, 2005; In Final Form: September 14, 2005

The hydration of the poly(oxyethylene) shell in polystyrene-*block*-poly(2-vinylpyridine)-*block*-poly(oxyethylene) micelles was investigated by monitoring the solvent relaxation response of a solvent-sensitive fluorophore (patman). It has been found that the relaxation occurs on the nanosecond time scale. Results for triblock copolymer micelles have been compared with those obtained for polystyrene-*block*-poly(2-vinylpyridine) micelles in order to evaluate the effect of the outer polyoxyethylene layer. Considerable pH-dependent changes in the hydration of poly(oxyethylene) units at the poly(2-vinylpyridine)/polyoxyethylene interface were observed. Additionally, the paper shows that the solvent relaxation technique is a suitable tool for studying polymeric nanoparticles and that the measurement of time-dependent half-width of the emission spectrum allows for estimation of the extent of relaxation process observed by a given experimental setup.

Introduction

Amphiphilic block polyelectrolyte micelles are interesting nanoparticles, which offer a number of potential applications. The high-molar-mass block copolymers with long hydrophobic blocks are usually insoluble in aqueous media, but the multimolecular micelles can be prepared indirectly, e.g., by dialysis.[1] Thanks to high practical importance of various micelle-based nanoparticles, the micellization of water-soluble polymers has been a subject of a number of studies.[2] While numerous studies of block polyelectrolyte micelles have been devoted to the micellization of AB or ABA copolymers, where A is a polyelectrolyte block and B is a nonpolar, water-insoluble block, only a limited number of papers have aimed at more complex micellizing systems, mainly at various mixtures of diblock copolymers, such as hybrid micelles,[3] Janus micelles,[4] or onion-type micelles.[5]

Recently, we studied the micellization of a triblock polyelectrolyte, polystyrene-*block*-poly(2-vinylpyridine)-*block*-poly(oxyethylene), PS−PVP−POE, in aqueous solutions.[6] Its self-assembling behavior is very interesting. Polystyrene, PS, is insoluble in aqueous media and forms micellar cores. Poly(oxyethylene), POE, is a water-soluble polymer and forms micellar shells. Poly(2-vinylpyridine), PVP, is protonized and soluble in acid solutions at pH lower than 4.8, whereas the deprotonized PVP that exists at higher pH is water-insoluble. The PS−PVP−POE micelle is thus a three-layer nanoparticle in which PVP blocks form the middle layer. This layer is either collapsed at high pH, thus PS−PVP−POE micelles resemble onion micelles formed by PS−PVP and PVP−POE diblock copolymers,[5] or partially protonized, swollen, and relatively flexible in acid media, thus PVP forms an inner shell between the PS core and the outer shell of POE.

We found that PS−PVP−POE micelles can be prepared both in acidic and in alkaline aqueous solutions by dialysis from 1,4-dioxane−methanol−water mixtures. Molar masses of micelles prepared in acidic and alkaline media differ, because the lengths of soluble and insoluble parts of chains also differ in respective media. The micelles can also be transferred from acid to alkaline media and vice versa; however, the transfer is usually accompanied by some aggregation, probably due to fairly reduced solubility of highly concentrated POE chains in micellar shells. Any mechanical shear of the solution, like shaking or stirring, accelerates the aggregation. The tendency to form aggregates is very pronounced in neutral and alkaline solutions, while in acid solutions, due to electrostatic repulsion between the micelles with protonized PVP inner shells, only little aggregation was observed.

In this paper, we employ a combination of standard (benchmark) polymer techniques with a fairly new and not very often used approach in polymer science, i.e., with a solvent relaxation method, which yields unique information on the dynamics of micellar shells, for the study of complex PS−PVP−POE micellar systems.

* To whom correspondence should be addressed.
[†] Charles University in Prague.
[‡] Jaroslav Heyrovský Institute of Physical Chemistry of the Academy of Sciences of the Czech Republic.

10.1021/jp053348v CCC: $30.25
Published on Web 11/09/2005

TABLE 1: Block Molar Masses of the Used Copolymers

copolymer	$M_n \times 10^{-3}$, g mol^{-1} PS	PVP	PEO	ref[a]
PS−POE	9.7		11.3	3a
PVP−POE		14.0	12.3	31
PS−PVP	36.0	34.0		5b
PS−PVP−POE[b]	14.1	12.3	35.0	

[a] Details on preparation and characterization. [b] Data provided by the manufacturer.

CHART 1

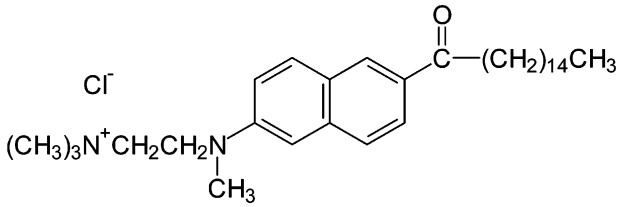

CHART 2

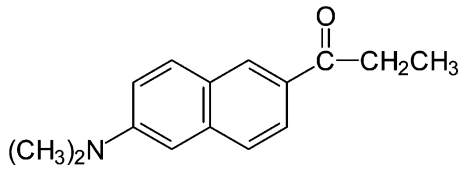

CHART 3

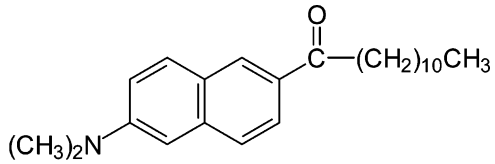

Experimental Section

Materials. *Copolymer Samples.* The triblock copolymer polystyrene-*block*-poly(2-vinylpyridine)-*block*-poly(ethylene oxide), PS−PVP−POE, with narrow distribution of molar masses and compositions was purchased from Polymer Source, Inc., Quebec, Canada, and used as obtained. The diblock copolymers polystyrene-*block*-poly(2-vinylpyridine), PS−PVP, polystyrene-*block*-poly(oxyethylene), PS−POE, and poly(2-vinylpyridine)-*block*-poly(oxyethylene), PVP−POE, were prepared at the University of Texas at Austin by living anionic polymerization. Molar masses of the used samples are summarized in Table 1 together with references concerning details on their synthesis and characterization.

Low-Molar-Mass Chemicals. 6-Hexadecanoyl-2-(((2-(trimethylammonium)ethyl)methyl)amino)naphthalene chloride, patman (Chart 1), 6-propionyl-2-dimethyl-aminonaphthalene, prodan (Chart 2), and 6-dodecanoyl-2-(dimethylamino)naphthalene, laurdan (Chart 3), were purchased from Molecular Probes, Eugene, OR. 1,4-Dioxane and methanol were purchased from Aldrich International and used without further purification. Deionized water was used in all experiments.

Techniques. *UV−vis Absorption.* UV−vis absorption spectra were measured in 1 cm quartz cuvettes using a Perkin-Elmer Lambda19 UV−Vis spectrophotometer.

Steady-State Fluorometry. Steady-state fluorescence spectra (i.e., corrected excitation and emission spectra) were recorded with a SPEX Fluorolog 3 fluorometer, USA, in a 1 cm quartz cuvette closed with a Teflon stopper.

Time-Resolved Fluorometry. A time-correlated single photon counting technique was used for measurements of fluorescence decays at different wavelengths spanning the emission spectra. The wavelength-dependent decays and steady-state intensities were used for the construction of TRES. The decays were recorded on a IBH 5000U time-resolved fluorometer (IBH, Glasgow, U.K.), equipped with an IBH NanoLED-03 excitation source (370 nm peak wavelength, 0.1 ns in full width in the half-maximum of the pulse, 1 MHz repetition rate) and a cooled Hamamatsu MCP photomultiplier. The deconvolution procedure was used to get the true fluorescence decays that were further fitted to multiexponential functions using the Marquardt−Levenberg nonlinear least-squares method. Low values of the χ^2 (close to 1.0) and random distribution of residuals were used as criteria for the quality of the fit.

The anisotropy measurements were carried out until a difference of at least 10 000 counts between the decay maxima with parallel and perpendicular position of polarizers, respectively, was reached with a dwell time 30 s. For the determination of the *G* factor, the decays were measured for 180 s.

Light Scattering Measurements. The light scattering setup (ALV, Langen, Germany), used for both static (SLS) and dynamic (DLS) measurements, consisted of a 633 nm He−Ne laser, an ALV CGS/8F goniometer, an ALV High QE APD detector and an ALV 5000/EPP multibit, multitau autocorrelator. The solutions for measurements were filtered through 0.45 μm Acrodisc filters. The measurements were carried out for different concentrations (0.1−3 mg/mL) and different angles at 20 °C. The measurements at low ionic strength solutions were performed in quartz cells.

The SLS data were treated by the standard Zimm method using the equation

$$\frac{4\pi^2 n_0^2 (\mathrm{d}n/\mathrm{d}c)^2}{\lambda^4 N_A} \frac{c}{R^{cor}(q,c)} = \frac{1 + (1/3)R_g^2 q^2}{M_w} + 2A_2 c \quad (1)$$

where n_0 is the refractive index of the solvent, (dn/dc) is the refractive index increment of the polymer with respect to the solvent, λ is the wavelength of the incident light, N_A is the Avogadro constant, $R^{cor}(q,c)$ is the corrected Rayleigh ratio which depends on the polymer concentration c and on the magnitude of the scattering vector, $q = (4\pi n_0/\lambda)\sin(\vartheta/2)$, where ϑ is scattering angle, M_w is the apparent weight average molar mass of scattering polymeric particles, A_2 is the "light-scattering-weighted" second virial coefficient of the concentration expansion, and R_g is the radius of gyration of scattering polymeric particles.

DLS data analysis was performed by fitting the measured normalized intensity autocorrelation function $g_2(t) = 1 + \beta|g_1(t)|^2$, where $g_1(t)$ is the electrical field correlation function, t is the lag time, and β is a factor accounting for deviation from the ideal correlation. An inverse Laplace transform of $g_1(t)$ with the aid of a constrained regularization algorithm (REPES) provides the distribution of relaxation times, $\tau A(\tau)$

$$g_1(t) = \int_{-\infty}^{\infty} \tau A(\tau) \exp(-t/\tau)\, \mathrm{d}\ln\tau \quad (2)$$

Diffusion coefficients were calculated from mean times of individual diffusion modes, $\langle\tau\rangle$, as $D = 1/(\langle\tau\rangle q^2)$. Hydrodynamic radii, R_H, were evaluated from the diffusion coefficients using the Stokes−Einstein formula.

Potentiometry. The pH measurements were performed with a Radiometer PHM 93 reference pH meter equipped with a PHC 3006 combined glass microelectrode.

Preparation and Characterization of Micelles. *Preparation of Micelles.* Both PS−PVP and PS−PVP−POE micelles were

TABLE 2: Molar Masses, Radii of Gyration, and Second Virial Coefficients of PS−PVP and PS−PVP−POE Micelles in 10^{-4} M HCl Solution

copolymer	$M_w \times 10^{-6}$, g mol^{-1}	R_g, nm	$A_2 \times 10^8$, mol L g^{-2}
PS−PVP	20.43	72.4	−0.7
PS−PVP−POE	0.71	25.5	24.5

prepared according to the same protocol. The copolymer was dissolved in a mixture of 1,4-dioxane (80 vol %) and methanol and slowly titrated with methanol under very mild stirring until 50% methanol content. Then the solution was carefully titrated with 0.01 M HCl aqueous solution until 50% water content. The next step was the dialysis of this solution against 0.01 M HCl, followed by the dialysis against a HCl solution of a desired concentration. During the final dialysis, the HCl solution was exchanged several times in the external bath to ensure removal of all traces of organic solvents. The concentration of polymers before the dialysis was 3 g/L. The concentrations of final solutions were calculated on the basis of measured volume changes during the dialysis.

PS−POE micelles were prepared by dissolving PS−POE in a mixture of 1,4-dioxane (80 vol %) and water (c = 3 g/L), and consequently stepwise dialyzed against mixtures containing 60, 40, and 20 vol % of dioxane to pure water.

POE−PVP micelles were prepared by dissolving POE−PVP in 0.01 M HCl solution and then adding an aliquot of 0.1 M NaOH for neutralization under vigorous stirring.

Characterization of PS−PVP and PS−PVP−POE Micelles by Light Scattering. The SLS measurements were performed in 10^{-4} M aqueous HCl solution.[7] Refractive index increments of copolymers, dn/dc, were calculated as the weight-average values based on copolymer composition and literature increments[8] for individual homopolymers. The obtained values of molar masses, M_w, radii of gyration, R_g, and second virial coefficients, A_2, for both PS−PVP and PS−PVP−POE micelles are summarized in Table 2.

Results and Discussion

Basic Characteristics of PS−PVP and PS−PVP−POE Micelles. Since the main goal of the study is the comparison of the behavior of PS−PVP−POE micelles with those formed by diblock PS−PVP, which is insoluble in aqueous solutions above pH 4.8 (i.e., when PVP is neutral), we restricted our PS−PVP−POE study to acid aqueous solutions (10^{-4}−10^{-1} M HCl) only.

The pH and ionic strength dependent behaviors of PS−PVP−POE micelles were studied in detail in separate papers.[6a,b] In this paper, we present only selected characteristics that we measured under identical conditions as solvent relaxation experiments and that are needed for interpretation of new results. Nevertheless, we have to mention briefly the most important general properties of the studied system that are necessary for an easy understanding of conclusions drawn from fluorescence measurements. Polystyrene is a strongly hydrophobic polymer and copolymers containing long PS blocks are insoluble in water. The multimolecular block copolymer micelles formed by copolymers containing insoluble hydrophobic PS and water-soluble (hydrophilic) blocks can be prepared indirectly in aqueous buffers, as follows: The copolymer is dissolved in a 1,4-dioxane-rich mixture with water, which is a mild selective solvent for the hydrophilic block, and reversible micelles form spontaneously. The micelles can be transferred in aqueous media by stepwise dialysis.[3a] When the content of water increases, the thermodynamic quality of the solvent for PS deteriorates. Critical micelle concentration decreases and the association number increases. At a certain critical composition dependent on the length of blocks, the solvent becomes very bad for PS and micellization equilibrium freezes. During further increase of the water content, the association number does not change any more. The unimer concentration (i.e., the critical micelle concentration (cmc)) drops to zero, the exchange of unimer chains between micelles stops, and micelles behave as kinetically frozen nanoparticles. In case of micelles with insoluble PS blocks, the cores are very compact, hard, and glassy at ambient temperatures because the glass transition temperature, T_g, of bulk PS is close to 100 °C.[8] The micelles effectively behave as inert PS nanospheres decorated by the water-soluble polymeric brush tethered to their surface. The micelles neither dissociate at low concentrations (they have no cmc) nor rearrange upon change of conditions. Their behavior is controlled by the properties of water-soluble chains only.

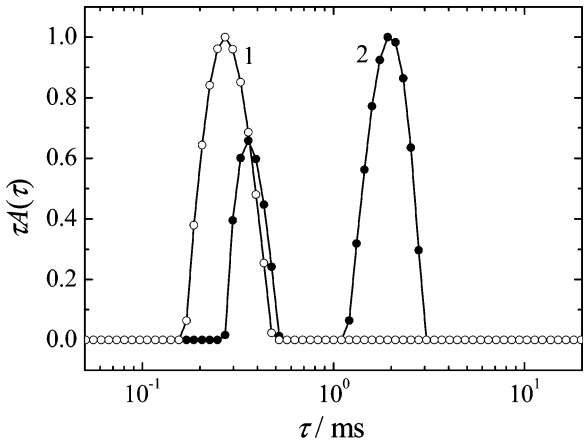

Figure 1. Distribution of DLS relaxation times for 0.09 g/L solutions of PS−PVP−POE micelles in 10^{-4} M (curve 1) and 10^{-1} M (curve 2) HCl (scattering angle 90°). Angular measurements prove the diffusion-controlled behavior of all observed modes.

However, the system studied here behaves a bit atypically. Thanks to the use of ternary mixtures during dialysis (1,4-dioxane−methanol−water), the association number of micelles prepared in acidic media is very low, ca. 12. In this case, the PS cores are not glassy (it was experimentally proven that T_g of thin films is lower than that of bulk polymers and the chains are more mobile).[9] Even though the exchange of chains among different micelles does not take place in our system (cmc is zero), the blocks in micellar cores may partially reorganize and a small fractions of micelles form micellar aggregates under conditions of decreased solubility of micellear shells due to a hindered hydration of shell-forming POE blocks. The solution and aggregation behaviors have been described and accounted for in detail in our recent paper.[6b]

As mentioned above, the PS−PVP−POE micelles in aqueous solutions (except in acidic solutions with very low ionic strength) tend to form large multimicellar aggregates with apparent hydrodynamic radii around 150 nm. The aggregation can be witnessed by DLS measurements, which are very sensitive to traces of large aggregates. Figure 1 shows the distribution of relaxation times measured by DLS. Curve 1 was obtained for micelles in a low ionic strength solution (10^{-4} M HCl). It shows only one fairly narrow band of relaxation times corresponding to single core−shell micelles. Curve 2, measured for the same polymer concentration at significantly higher ionic strength (in a 0.1 M HCl solution), is bimodal and indicates the presence of micellar aggregates. Angular measurements prove that both

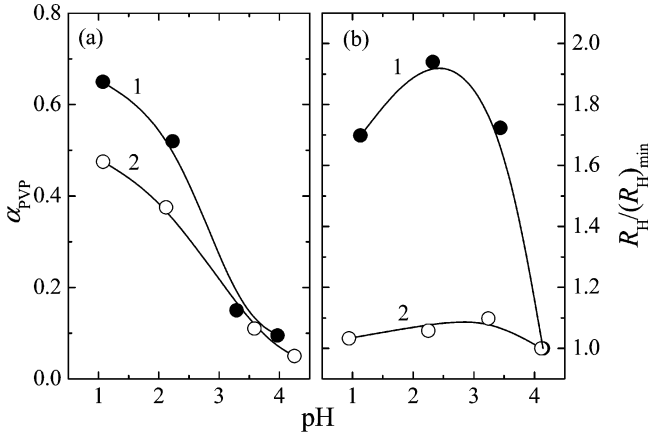

Figure 2. (a) Degree of protonization, α_{PVP}, of the PVP shell-forming blocks in PS−PVP (curve 1) and PS−PVP−POE (curve 2) micelles as a function of pH of the solution. (b) Relative hydrodynamic radius, $R_H/(R_H)_{min}$, of PS−PVP (curve 1) and PS−PVP−POE (curve 2) micelles as a function of pH of the solution. $(R_H)_{min}$ values for PS−PVP and PS−PVP−POE micelles were 83 and 28 nm, respectively.

modes correspond to the diffusion-controlled motion. Although the presence of aggregates in the studied system strongly affects the light scattering data, it almost does not influence the solvent relaxation behavior around patman probes (except that for a fairly low pH 1). This observation may be rationalized as follows: First, the static light scattering measurement yields the weight-average molar mass and the *z*-average radius of gyration, and dynamic light scattering yields the *z*-average-based hydrodynamic radius. Hence both techniques are very sensitive to traces of large particles in the solution. Second, the micellization equilibrium is kinetically frozen. Although the aggregation requires minor rearrangement of PS blocks in cores, it occurs without redistribution of unimers among different micelles forming one aggregate.[6b] Hence, the basic structure of individual micelles in aggregates remains preserved. Therefore the fluorescent probes embedded in shells of aggregated and single micelles (close to the PVP/POE interface—see later) experience a similar microenvironment. Nevertheless, a major aggregation at low pH does affect the solvent relaxation as will be shown below.

The basic properties of the studied system depend strongly on the protonization of PVP blocks. The degree of protonation of PVP blocks, α_{PVP}, was measured by alkalimetric titration using the method described in our earlier papers.[10] The α_{PVP} of poly(2-vinylpyridine) in both PS−PVP (curve 1) and PS−PVP−POE (curve 2) micelles in HCl aqueous solutions is plotted in Figure 2a as a function of bulk pH of the solution. The results indicate that the protonization of PVP blocks in the PS−PVP−POE inner shell, surrounded by the outer shell of hydrated POE, is suppressed: At pH 1, α_{PVP} is only 0.48, i.e., it is substantially lower than the value found for the PVP shell in PS−PVP micelles ($\alpha_{PVP} = 0.65$), in which PVP blocks are exposed to the aqueous solvent.

The degree of protonization affects the hydrodynamic radius of micelles. Figure 2b shows the pH dependence of apparent *z*-average-based hydrodynamic radii of PS−PVP (curve 1) and PS−PVP−POE micelles (curve 2), relative to the values measured in 10^{-4} M HCl, $(R_H^{app})_{min}$, which are 83 nm for PS−PVP and 28 nm for PS−PVP−POE. Since the electrostatic repulsion between positively charged segments of poly(2-vinylpyridine) results in more stretched conformations of protonized PVP chains compared to neutral PVP chains, the apparent hydrodynamic radius, R_H^{app}, of micelles with PVP shells depends strongly on α_{PVP}. Therefore R_H^{app} of PS−PVP micelles increases with decreasing pH until pH around 2, where the dependence passes a maximum. A slight decrease in R_H^{app} after further addition of HCl is due to the electrostatic screening effect of H_3O^+ and Cl^- ions present in the shell. In the case of PS−PVP−POE micelles, both the protonization and the consequent expansion of little protonized PVP inner shells are suppressed by the outer POE shell and R_H^{app} is only slightly affected by pH, as the size of the micelles reflects mainly the conformations of POE chains.

Basic Premises on the Solvent Relaxation Process in Micellar Shells. The solvent relaxation method belongs to the category of time-resolved fluorescence techniques. This particular technique monitors the time-dependent shift in fluorescence emission spectra of probes with large differences between dipole moments before and after excitation and reports on the micropolarity and microviscosity of the probe environment. It is fairly popular in biochemistry and has been frequently used in membrane research,[11−15] but its use in polymer research is rather limited. We use the solvent relaxation technique to study changes in the hydration of poly(oxyethylene) (POE) chains in diblock and triblock copolymer micelles. Some work dealing with swollen POE-based copolymers,[16] amphiphilic starlike macromolecules,[17a] liquid oligo(ethylenoxide)s,[17b] surfactants,[17c] and polymer micelles[18a−e] has already been published. However, the quantification of the extent of observed relaxation processes was either missing or insufficient in the published papers.

The reorientational motion of solvent molecules after excitation in nonviscous isotropic polar solvents occurs in subpicosecond time range and leads to minimization of the overall energy (Gibbs function). Such fast relaxation process can be studied thanks to the development of ultrafast spectroscopic methods in past decades. The relaxation starts with a fast inertial (libration) motion (in 50−500 fs time range) and continues as a slower rotation and translation motions on the picosecond and subnanosecond time scales.[19,20] The relaxation is usually slowed by the presence of macromolecular components or other organized structures in the studied system. E.g., for probes embedded in phospholipid bilayers, a considerable part of the process proceeds in the range of nanoseconds.[21]

In this paper, we study solvent relaxation in solutions of self-assembled polymer systems by time-correlated single photon counting (TCSPC) technique with subnanosecond time resolution. There are significant differences between relaxations of "free" and "micelle-bound" water molecules. In pure water, the process is fast and isotropic in all three dimensions. The solutions of polymeric micelles contain large self-assembled polymeric particles, smaller fluorophores (e.g., fluorescent surfactant molecules of patman), and small water molecules. The probes are more or less firmly bound to large nanoparticles, because they are embedded in hairy shells of polymeric micelles. Properties of the shell, i.e., the density and flexibility of shell-forming chains, concentrations of low-molar-mass molecules, and the effective hydrophobicity change in the radial direction (mainly in systems with shells formed by weak polyelectrolytes).[22a] The studied relaxation process should be treated as an anisotropic one-dimensional (radial) problem with respect to the axis connecting the center of gravity of the nanoparticle and the excited fluorophore, since, as mentioned above, there exists a gradient in almost all properties of the system as depicted in Scheme 1 which is based on results of our Monte Carlo simulations for a diblock copolymer micelles with polyelectrolyte-shell-forming blocks.[22b]

At present, it is practically impossible to analyze and interpret all details of the fluorescence response of probes embedded in

SCHEME 1: Diblock Copolymer (Block Polyelectrolyte) Micelle with Embedded Patman (White P-Marked Sphere with Tail)[a]

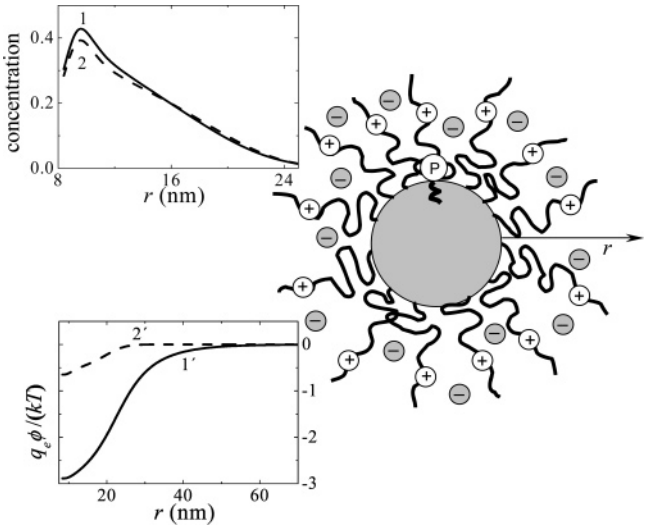

[a] The plots show the gradient in micellar properties: the electrostatic potential and segment concentration decrease in the radial direction. Lower inset: The reduced electrostatic potential, i.e., $q_e\phi(r)/kT$, where q_e is the elementary charge, $\phi(r)$ the electrostatic potential, k the Boltzmann constant, and T the temperature, as a function of the distance from the micellar center, r, for dilute aqueous solution of micelles at pH close to the effective dissociation constant of the weak polyelectrolyte, pK_A, and $I = 0.001$ and 0.1, the full curve 1′ and dashed curve 2′, respectively (data from ref 22). Upper inset. Curves 1 and 2 show corresponding concentration profiles of PMA in the shell for comparison of the range of the electrostatic interaction with the geometric size of micelles. The plots are based on results of our earlier studies for polystyrene-*block*-poly(methacrylic acidic) micelles.[22] For the weak polybase such as PVP, the curves are schematically the same, only the sign of the potential is opposite. The simulated density profile is not monotonic and rises slightly at short distances from the PS core. This is an artifact of the simulation model, which assumes that the surface of the PS core is absolutely impenetrable for the shell-forming chains. In real micelles, the uncharged parts of the shell-forming chains are slightly intermixed with PS chains at the interfacial region and the shell density decreases monotonically in the radial direction.

micellar shells, and it is why some simplifying assumptions are necessary. In the first approximation, we assume that the fluorescent response on the nanosecond time scale is mostly due to reorientation of water molecules in the vicinity of the fluorophore. The properties of individual water molecules in the shell change only little at distances comparable with the size of the fluorophore and small differences may be neglected although the gradient in shell properties does affect the relaxation behavior; i.e., we take into account only the radial position of the probe. Further, we assume that (i) for a moderately hydrophobic probe, which is embedded in hydrated domains, the shell-forming blocks influence the relaxation behavior indirectly via interaction with bound water molecules. A considerable fraction of water molecules in micellar shells is engaged in the hydration of structural units of polymer chains (bound water) and their movement is considerably slowed and influenced by segmental dynamics of shell-forming blocks. (ii) If a strongly nonpolar fluorophore is trapped in dehydrated or only little hydrated domains of the polymeric nanostructure, than the slowly moving polymer chains control the observed relaxation directly.

Solvent Relaxation Studies in Shells of Diblock Copolymer Micelles. At first, we studied the solvent relaxation in solutions of diblock copolymer micelles. A commercially available

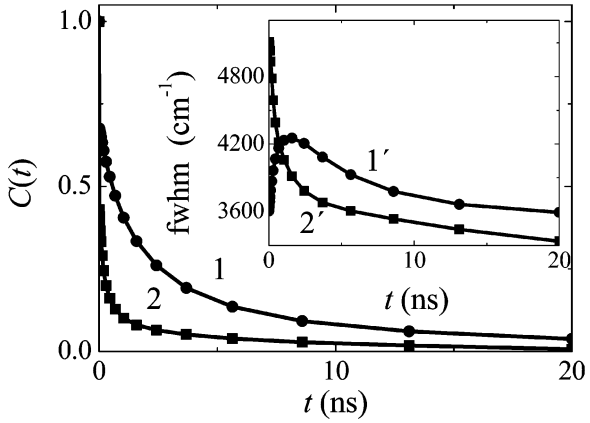

Figure 3. Time-resolved Stokes shift, $C(t)$, of patman in PS−POE micelles (curve 1) and PS−PVP micelles (curve 2). Inset: Time-dependent half-width of the time-resolved emission spectra of patman in PS−POE micelles (curve 1′) and in PS−PVP micelles (curve 2′).

polarity-sensitive probe, patman, whose behavior is known from studies in phospolipid bilayers[11−15,23−26] was added to aqueous solutions of polystyrene-*block*-polyoxyethylene (PS−POE) micelles. The probe binds strongly to micelles because its hydrophobic aliphatic chain has a strong affinity to the nonpolar PS core. Because of the permanent positive charge at the nitrogen atom and a fairly long aliphatic tail (see Chart 1), the fluorescent headgroup of the surfactant dye is supposed to be localized in POE shell close to the core/shell interface. The assumed localization has been supported by time-resolved anisotropy measurements (see later).

To get an idea "where the relaxation process starts on the energy scale", i.e., to estimate the energy level of the maximum disturbed system immediately upon excitation (before the relaxation starts) and the frequency of the emission maximum at the "time zero", we performed the estimation of the "time zero" frequency according to Fee and Maroncelli.[19,27] This procedure requires the knowledge of the absorption spectrum of the fluorophore in the studied media and its absorption and emission spectra in a particular nonpolar reference solvent. For patman, which is charged and insoluble in nonpolar solvents, we use spectra of an analogous compound, prodan (because their spectra in a series of common solvents are almost identical). Then the time-dependent fluorescence decays at different wavelengths were measured and the time-dependent emission spectra (TRES) were reconstructed. This allows a plot of the time-dependent Stokes shift, i.e., the frequency of the emission maximum, $\nu_{max}(t)$ as a function of time. The entire Stokes shift, i.e., the difference between the positions of emission maxima at the "time zero" corresponding to the maximum perturbed state and at the "infinite time" corresponding to the fully relaxed state, i.e., $\Delta\nu_{max} = \nu_{max}(0) - \nu_{max}(\infty)$ characterizes the micropolarity of the fluorophore environment. For monitoring the relaxation process, we use the correlation function, $C(t)$, corresponding to the normalized time-dependent Stokes shift.

$$C(t) = \frac{\nu_{max}(t) - \nu_{max}(\infty)}{\nu_{max}(0) - \nu_{max}(\infty)} \qquad (3)$$

The comparison of the span of measured values with that based on the "time zero" estimation suggests that at least 70% of the reorientation motion has been displayed by monitoring the fluorescence behavior of micelle-embedded patman with our instrumental setup. Figure 3 (curve 1) depicts the relaxation correlation function monitored by patman bound to diblock PS−POE micelles.

TABLE 3: Stokes Shifts and Relaxation Times for Patman and Laurdan in Various Copolymer Micelles and at Different pH Values

copolymer	dye	Stokes shift (cm^{-1})	t_1 (ns)[a]	A_1[a]	t_2 (ns)[a]	A_2[a]	t_3 (ns)[a]	A_3[a]	$\langle t \rangle$ (ns)[b]
PS−POE (water)	patman	3390	4.8	0.4	0.2	0.3	<0.2	0.3	2.7 ± 0.3
PS−POE (pH 2)	patman	3430	3.5	0.2	1.0	0.4	<0.2	0.4	1.0 ± 0.1
PS−POE (pH 12)	patman	3550	3.3	0.3	0.7	0.3	<0.2	0.4	1.2 ± 0.1
PS−PVP (pH 2)	patman	3320	5.0	0.1	0.2	0.3	<0.2	0.6	0.7 ± 0.1
PS−PVP−POE (pH2)	patman	3300	3.9	0.3	0.8	0.4	<0.2	0.3	1.4 ± 0.1
PS−PVP−POE (pH3)	patman	2130	5.1	0.5	0.5	0.2	<0.2	0.3	3.3 ± 0.3
PS−PVP−POE (pH4)[c]	patman	1850	11.0	0.4	0.7	0.2	<0.2	0.4	>4.1
PS−PVP−POE (pH12)[c]	patman	1630	9.1	0.5	0.8	0.2	<0.2	0.3	>3.9
PS−POE (water)[c]	laurdan	1150	11.3	0.7	1.1	0.3			>6.6

[a] Parameters of the three-exponential fit of the correlation curve: $C(t) = \sum_1^3 A_i e^{-t/t_i}$. [b] Integration time: $\langle t \rangle = \int_0^\infty C(t)\, dt$. [c] The values of the Stokes shifts are estimated from the three-exponential fit of the emission maximum shift and extrapolating to infinity.

The time-dependent half-width of the emission spectra was also measured. Whereas the time-resolved red shift of the emission spectrum is commonly used for monitoring the solvent response, the time-dependent change of the half-width provides rough, but useful, information on the extent of the observed process. The experiments carried out in supercooled liquids[28] and in phospholipid bilayers using patman[11,26] have shown that the half-width passes a maximum, which is in a good agreement with the idea of nonuniform spatial distribution of solvent response times.[28,29] It has been shown that in homogeneous systems of low-molar-mass molecules, the half-width always decays monotonically. In a spatially inhomogeneous system (it applies also to inhomogeneity on the nanometer length scale), the relaxation behavior is different. Since the properties of the system vary in space, individual fluorophores distributed in the system are nonequivalent and their solvent shells respond with different rates to local electric field. This inhomogeneity gives rise to a new phenomenon, which reflects the time distribution of phases of relaxations of individual solvation shells during the relaxation. The observed transient inhomogeneity increases significantly, and the time dependence of the observed half-width passes a pronounced maximum.

The time dependence of the half-width of the emission spectra in the studied micellar systems provides information on whether the entire response or merely part of it was captured within the time window of the experiment. If only a decrease in the half-width is observed, the early part of the relaxation process is beyond the time resolution of the TCSPC equipment. In contrast, if only an increase is observed, the process is fairly slow under given conditions and the lifetime of the used fluorophore is not long enough for monitoring the overall relaxation process. The time-dependent behavior of the half-widths is depicted in the insert in Figure 3 (curve 1′). The curve with a well-pronounced maximum supports the conclusion based on the "time zero" frequency estimate that the used experimental setup detects ca. 70% of the total response. Therefore we assume that only 30% of the entire relaxation is beyond the time resolution of the TCSPC equipment and a major part of the dynamics due to relaxation of bound water molecules engaged in the solvation sphere of POE units occurs in the nanosecond time range (see Table 3) and can be monitored by time-resolved fluorescence measurement.

To get an idea where the dye is located in the micelle, we performed time-resolved anisotropy measurements. However, it must be kept in mind that the anisotropy measurements for polarity-sensitive probes, such as patman, provide only rough and indirect information on the viscosity of the microenvironment of the probe. It has been recognized that the experimental anisotropy of polarity-sensitive probes is not a good tool for monitoring the microviscosity, since both the reorientational time

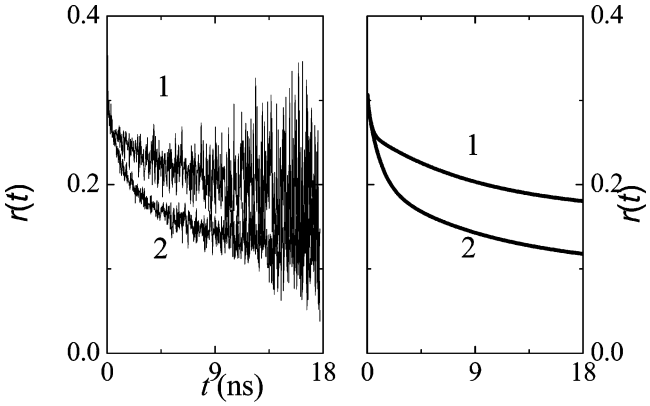

Figure 4. (left) Time-resolved anisotropy, $r(t)$, of patman in the PS−POE micelles at different emission wavelengths, 430 nm (curve 1) and 510 nm (curve 2). (right) Two-exponential fits of time-resolved anisotropy decays at 430 nm (curve 1) and 510 nm (curve 2).

TABLE 4: Parameters for Anisotropy Decays of PS−POE Micelles in Water at 430 and 510 nm

wavelength (nm)	$r(\infty)$	α_1	τ_1 (nm)	α_2	τ_2 (nm)
430	0.24	0.92	2.9 ± 0.5	0.08	0.07 ± 0.01
510	0.08	0.91	8.1 ± 1.5	0.09	0.8 ± 0.1

and the residual anisotropy are influenced by solvent relaxation and are wavelength-dependent.[30] The measurement of decay curves was performed at different wavelengths. Two curves, at 430 and 510 nm, are shown in Figure 4. Because the mean rotation correlation times are comparable with the mean fluorescence lifetime, a fairly high scatter of experimental points is observed at later times. However the statistics at early times are reasonably high and provide reliable and accurate correlation times. All decays show a relatively slow process and suggest that the dye is localized in constrained and considerably rigid domains. Parameters of the time-resolved anisotropy decays at 430 and 510 nm are summarized in Table 4. The measurements for longer emission wavelengths monitor the behavior of more relaxed states and the observed decays reflect higher extents of depolarization. Since the average fluorescence lifetime increases with wavelength, a lower residual anisotropy is also observed in the red part of the spectrum. In the studied nanoheterogeneous and nanoanisotropic system with properties depending on the radial direction (possibly including also the micellar electric potential), the excitation-induced change in the dipole moment of the probe may affect not only its average position and orientation but also its translation and rotation diffusion with respect to the radial direction (i.e., to the nanoparticle). Even though the time-resolved anisotropy and spectral shift are correlated, the present level of knowledge does not allow going into detail.

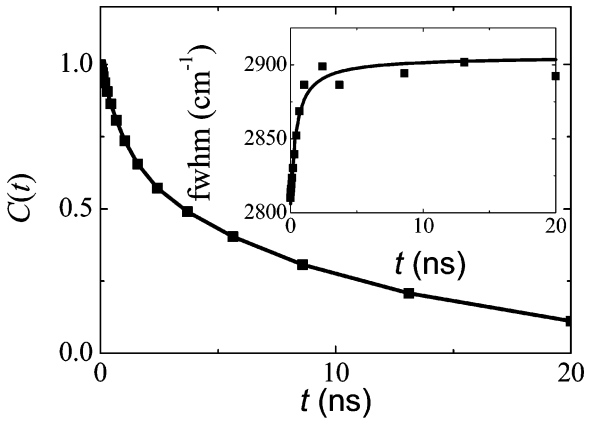

Figure 5. Time-resolved Stokes shift, $C(t)$, of laurdan in PS−POE micelles. Inset: Time-dependent half-width of time-resolved emission spectra of laurdan in PS−POE micelles.

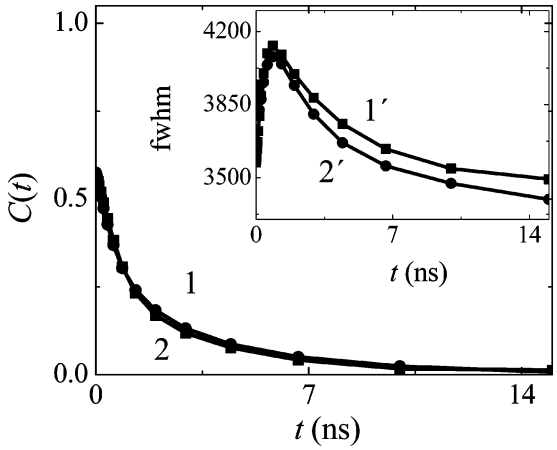

Figure 6. Time-resolved Stokes shift, $C(t)$, of patman in PS−POE micelles in alkaline solution, 0.01 M NaOH, (curve 1) and in acid solution, 0.01 M HCl (curve 2). (inset) Time-dependent half-width of the time-resolved emission spectra of patman in 0.01 M NaOH (curve 1′) and in 0.01 M HCl (curve 2′).

To support our idea of patman location, PS−POE micelles were labeled also by laurdan that has also an aliphatic chain (slightly shorter as compared with patman) and the same fluorescent headgroup, but it misses the permanent charge at the nitrogen atom. The correlation function, $C(t)$ and time-dependent half-width for measurement with laurdan are displayed in Figure 5. Both curves suggest that the solvent relaxation dynamics is much slower than that of patman. According to the "time-zero" estimation, there is nearly no contribution of the fast process beyond experimental resolution. This observation provides proof that the fluorescent headgroup is embedded in the core, which is supported also by the small value of the Stokes shift (Table 3).

As we intend to study the pH-dependent hydration of POE in triblock copolymer micelles (see later), we measured the solvent relaxation for patman embedded in PS−POE micelles both in acidic (0.01 M HCl) and alkaline (0.01 M NaOH) solutions for comparison. The relaxation is a bit faster in basic media, but the differences are only marginal for such large pH span (Figure 6). The difference in relaxation times is a bit larger than experimental errors of the spectral reconstruction based on total analysis of the set of measured curves, but we may conclude that the dye itself does not exhibit any major pH-dependent changes after binding to micelles. Since the shell-forming blocks are not charged, we do not assume any significant changes in the probe location. The changes are probably caused by slightly different mobility of water molecules in the shell at different pH, but since the changes are small, we prefer to avoid any unjustified speculations for the time being. In all cases, we observe an initial fast relaxation. The lower limit of the apparatus, as well as the experimental error of evaluation of individual decay curves, is below 0.2 ns. Hence the shortest experimental correlation time is 0.2 ns, but we assume that the relaxation at early times comprises contributions of various (already mentioned) faster processes.

The solvent relaxation was also studied in polystyrene-*block*-poly(2-vinylpyridine), PS−PVP, micelles in 0.01 M HCl solution. The micelles are stable in acidic solutions where they are positively charged. Nevertheless, our earlier studies suggest that the poly(2-vinylpyridine) layer partially collapses around the core because PVP is only little protonized close to the nonpolar PS core.[31] A fairly high value of the residual anisotropy (around 0.2) measured at the maximum emission intensity (467 nm) suggests that patman is embedded in a relatively dense part of the shell close to PS/PVP interface; i.e., its location in PS−PVP micelles is similar to that in PS−POE micelles.

However the solvent relaxation in patman-labeled PS−PVP micelles is considerably faster than that in PS−POE micelles (Figure 3, curves 2 and 2′). It indicates that more free water molecules are engaged in the energy minimization than in the case of PS−POE micelles. The shell-forming PVP chains are electrically charged and fairly stretched at the shell periphery at pH 2 and this may be the main cause of differences in rates of relaxation processes in PS−PVP and PS−POE micelles. The hydrodynamic radius of PS−PVP micelles is nearly two times larger at pH 1 than at pH 4 where the degree of protonization is very low and nearly all PVP is collapsed around the core. The charged PVP shell is on average less dense and evidently more hydrated than the POE shell. We expect that solvent molecules in the PVP shell are less structured not only than those in POE shell but also than the bulk water. It is a recognized fact that the hydration of large ions and therefore also large charged $PVPH^+$ groups results in a net water structure-breaking effect.[32] Apparently not all water molecules are engaged in the solvation of PVP or $PVPH^+$ units, but they behave as effectively free. The "time zero" estimation suggests that ca. 60% of the relaxation processes is beyond the experimental resolution. This conclusion is supported also by monitoring the full width at half-maximum (fwhm) that shows only the decrease.

In both PS−POE and PS−PVP micellar systems, the fluorescent surfactant, patman, is embedded in fairly concentrated parts of the shell where the mobility of chains is strongly restricted. The differences in rates of the relaxation processes are mostly due to different solvation of the shell-forming chains and different structure of water in both types of shells. From the geometrical point of view, poly(oxyethylene) chains easily incorporate into icelike structure and the presence of both the hydrogen-bonding oxygen atom and hydrophobic $-CH_2-$ group promotes the structure formation. The water-structure-supporting character of POE is generally recognized and was confirmed by different experiments.[33−37] The ice-like-structured water molecules bound to fairly concentrated and geometrically constrained (and hence only little mobile) POE chains in the inner part of micellar shells are responsible for slow relaxations in PS−POE micelles.

Solvent Relaxation Study in Shells of Triblock Copolymer Micelles. In this and in our earlier studies,[6a,b] we have shown that the pH-dependent behavior of micelles formed by triblock copolymer PS−PVP−POE is fairly complex. While DLS measurement reflects the overall size changes and is sensitive

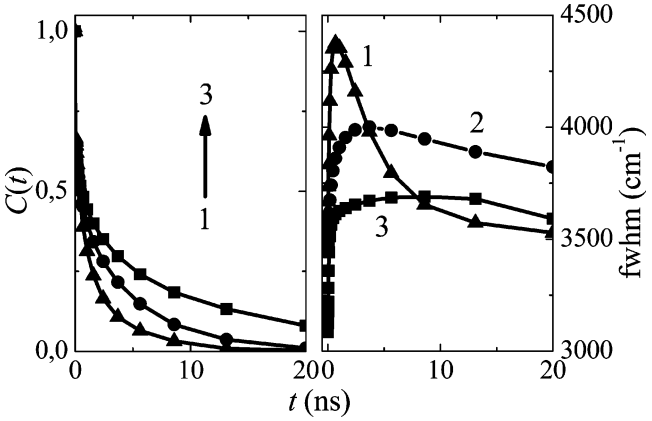

Figure 7. (left) Time-resolved Stokes shift, $C(t)$, of patman in PS−PVP−POE micelles at different pH values: pH 2 (curve 1), pH 3 (curve 2), pH 4 (curve 3). (right) Time-dependent half-widths of the time-resolved emission spectra of patman in PS−PVP−POE micelles at pH 2 (curve 1), pH 3 (curve 2), and pH 4 (curve 3).

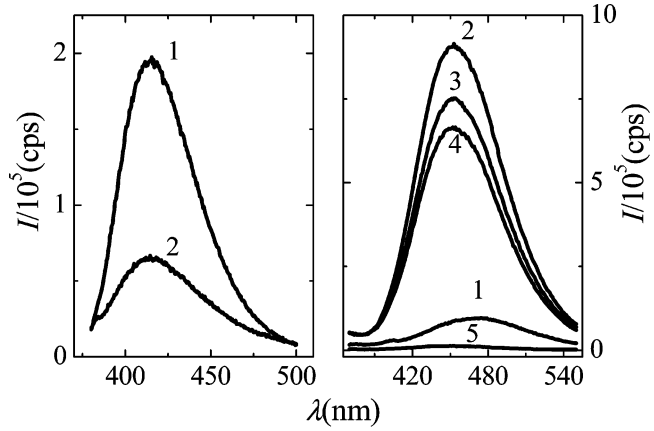

Figure 8. (left) Emission spectra of patman (1.8×10^{-6} mol/L) in dioxane before (curve 1) and after (curve 2) adding of poly(2-vinylpiridine). The concentration of PVP in 1,4-dioxane was 5.3 g/L. (right) Emission spectra of patman in the acidic (0.01 M HCl) aqueous solution of protonized PVP−POE (curve 1), i.e., before the micelles are formed, patman is strongly quenched. During alkalimetric titration of PVP−POE with 0.1 M NaOH, PVP is deprotonized and micelles are formed. The formation of micelles is manifested by blue shift of the maxima and increase in emission intensity (curve 2). Curves 3, 4, and 5 show the decrease in fluorescent intensity due to patman quenching by deprotonized PVP. The measurements were performed 15 min (curve 3), 40 min (curve 4), and 17 h (curve 5) after the micelles had been formed.

to the presence of traces of aggregates, the time-resolved fluorescence measurement with patman reflects interesting behavior of the middle part of the shell, because it monitors the changes in the state of the PVP/POE interface. As the micelles aggregate only little in the pH range 2−4, but the aggregation increases significantly in strongly acidic media around pH 1, we divided the discussion of relaxation measurements in two parts. We start with nonaggregated systems. The normalized time-dependent Stokes shifts and time-dependent half-width of patman spectra (pH 2−4) are presented in Figure 7. The solvent relaxation measurements show that although changes in $(R_H)^{app}$ are fairly small (DLS data for PS−PVP−POE micelles indicate that the POE layer suppresses the effects of bulk pH on $(R_H)^{app}$), the protonization and swelling of a PVP middle layer strongly affects the behavior of water in the hydration sphere of POE close to the PVP/POE interface.

For a correct interpretation of the pH dependence of relaxation rates, several facts have to be taken into account: At first, it has to be stressed that patman is believed to reside at the PVP/POE interface. The measurements do not preclude small changes in the patman position with pH, but the following arguments support our assumption that only negligible pH-induced displacements in the radial direction can be expected.

(i) The hydrophobic chain of patman tends to bury in nonpolar parts of micellar structures (PS or nonprotonized PVP) whereas the charged fluorophore headgroup prefers polar environment. The length of the hydrophobic 16 carbon chain together with the rigid naphthalene-derived cycle is fairly limited and does not allow large displacements.

(ii) At low pH, the shell-forming PVP chains are partially protonized and we assume that the aliphatic chain of patman, which prefers the PS core (and partially also nonprotonized PVP) to partially protonized PVP, tries to pull the fluorophore closer to the core, but the headgroup, which bears the same positive charge as the protonized PVP units, prefers the location in the POE outer shell to the PVP middle shell due to electrostatic repulsion. Therefore both effects more or less compensate for each other and the location of patman does not almost vary with pH. This assumption is supported by the experimental observation that in low pH solutions (below pH 4), both $C(t)$ and fwhm show similar relaxation behavior as that in PS−POE micelles (different from micelles with protonized PVP shells). This indicates the same microenvironment of patman in PS−PVP−POE micelles as in PS−POE micelles and supports the location of the headgroup in POE layer.

(iii) To yield more consistent view and to quantify viscosity of the fluorophore microenvironment (i.e., the flexibility of solvated chains in the place where the fluorophore is located), the time-resolved anisotropy measurements were performed for pH 2 and 4. The decays are relatively slow, i.e., a bit slower than decays in PS−POE micelles (cf. Figure 4), indicating fairly high rigidity of the microenvironment (not shown).

(iv) Auxiliary measurements show that deprotonized PVP chains quench patman fluorescence. This can be observed directly either in the dioxane solution or in the alkaline solution of PVP−POE micelles in the presence of patman (Figure 8). Since there is no observable decrease in fluorescence intensity in triblock copolymer micelles, we consider that patman is not in a direct contact with deprotonized PVP.

(v) Last, but not least, the measurements with increasing ionic strength of the solution at pH 2 did not show any effect on the solvent relaxation, which precludes significant displacement of patman in the radial direction out of the interfacial region due to either increasing protonization or screening of electrostatic repulsion (at higher salt concentrations).

The correlation curves as well as the shape of the time-dependent half-width clearly suggest that the average mobility of the solvent molecules around patman decreases with increasing pH. While for pH 2−3, the fast time resolution of the instrumental setup is the main limiting factor, at pH 4, slow processes are observed, the study of which is limited by the lifetime of the dye. We observe that the fast (experimentally unresolved) contribution decreases with increasing pH and the nanosecond process, which is considered to be caused by the reorganization of bound water molecules engaged in the solvation sphere of POE, prevails. At pH 4, we cannot monitor the end of the relaxation because the second contribution is too slow. The segmental motion and reorganization of the dehydrated polymer chains are assumed to be responsible for the slow relaxation.

We can summarize that all comparative measurements for PS−POE, PS−PVP, PVP−POE, and PS−PVP−POE micelles

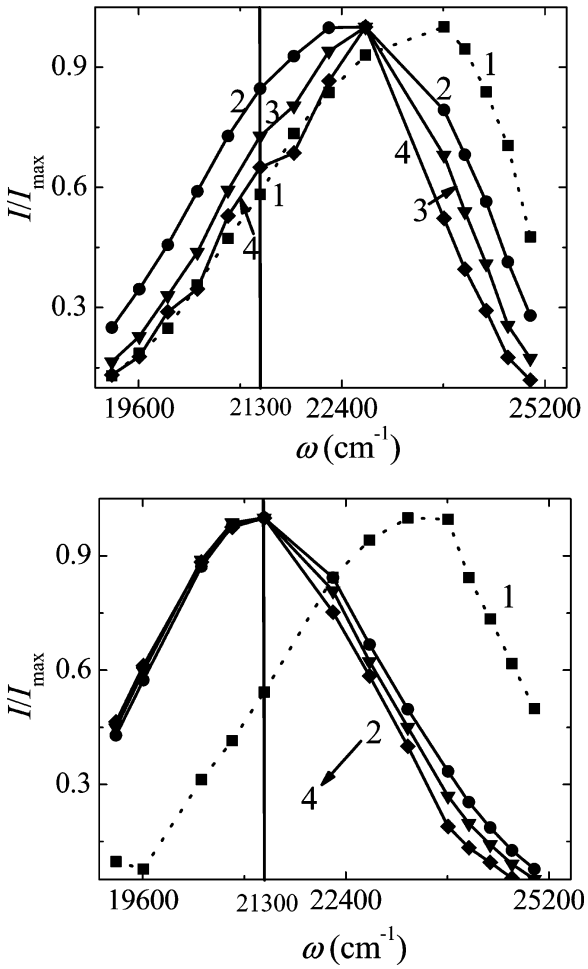

Figure 9. Normalized time-resolved emission spectra of patman in PS−PVP−POE micelles at pH 1 (a) and pH 2 (b) at "time zero" (curve 1), 1 ns (curve 2), 13 ns (curve 3), and 20 ns (curve 4) after the excitation.

outlined above suggest that, in PS−PVP−POE micelles, patman probes are preferentially localized in the POE part of the shell, very close to the PVP/POE interface, and their position is only little influenced by the bulk pH. This deduction is only indirect, but it supported by a number of independent pieces of information that fit together and support each other. However, the mobility of water molecules surrounding patman is affected by the pH-dependent protonization of PVP blocks. This conclusion is based on an indubitable experimental observation. The indirect pH influence may be accounted for as follows: Because the protonization increases with decreasing pH and increasing distance from the PS core (see Scheme 1), at low pH, an important concentration of charged $PVPH^+$ groups exists fairly close to the fluorescent headgroups of patman at the PVP/POE interface. As already mentioned, the hydration of relatively large ions and hence also of large charged $PVPH^+$ groups results in a significant perturbation of the water structure.[32] It is why more mobile water molecules exist close to the fluorofore and may participate at the solvent relaxation process at low pH 2. At pH 3 and 4, the PVP/POE interface is more dehydrated and water molecules are engaged in POE-promoted structure formation.[33] Therefore the overall solvent relaxation slows down with increasing pH.

The relaxation behavior at pH 1 is very interesting, but it is difficult to analyze it in detail. The relaxation is very fast, i.e., approximately 60% of the fast relaxation dynamics is beyond the experimental resolution. This fact suggests an important contribution of free water molecules to the entire solvent relaxation. The normalized time-resolved spectra of patman embedded in the shell of PS−PVP−POE micelles at pH 1 are depicted in Figure 9a. Figure 9b shows the patman time-resolved spectra at pH 2 for comparison. While the emission bands of partially relaxed states are monomodal at pH 2 with maximum around 21 300 cm^{-1}, the partially relaxed states at pH 1 show maxima close to 22 400 cm^{-1} with a well-pronounced shoulder close to 21 300 cm^{-1}, which appears at long times. The bimodal character of the emission spectrum does not allow the evaluation of the time-resolved Stokes shift without additional information. We believe that this complex relaxation behavior is a result of micellar aggregation, and in analogy with the regular behavior at pH 2, we attribute the maximum around 21 300 cm^{-1} to the microenvironment analogous to that of patman in nonaggregated micelles. In any case, the emission spectra indicate two different types of patman microenvironments in micellar shells, the first one in single micelles and the second in micellar aggregates, and demonstrate the complexity of the solvent response in heterogeneous systems.

Conclusions

The presented results clearly demonstrate that the POE layer in PS−PVP−POE micelles hinders the protonization of monomeric units of the middle PVP block. DLS measurements show that it suppresses the changes of the hydrodynamic radius of micelles due to changes in bulk pH. The solvent relaxation technique yields a closer insight in the dynamical behavior of the shell-forming blocks.

First, it has been proved that the solvent relaxation measurement using a TCSPC setup with nanosecond resolution is a useful tool for studying the structure, segmental dynamics, and solvation of shell-forming blocks in polymer micelles since the main reorientation of solvent molecules occurs on the nanosecond time scale.

Second, it has been shown that the contemporary measurement of the correlation function together with the time dependent half-width not only allows for evaluation of the rate of solvent relaxation in spatially inhomogeneous systems but also shows the extent of these processes that occurs in the time window of the method, i.e., lifetime of the excited state of the fluorophore and the time resolution of the instrumental setup used.

Third, the solvent relaxation technique revealed that the solvent response rate at the PVP/POE interface depends strongly on the degree of protonization of poly(2-vinylpyridine). With increasing pH, the solvent response slows down, which suggests less freely moving water molecules in the POE layer that are exchanged by the water molecules bound in the hydration sphere of the POE. At pH 4, the very slow process suggests the nearly dehydrated PVP/POE interface. The monitoring of time-dependent half-widths nicely supports the conclusions drawn from the analysis of the $C(t)$ correlation function.

Acknowledgment. M.H. and J.H. acknowledge the support of the Czech Academy of Sciences via Grant No. A400400503. M.Š. and K.P. acknowledge the support of the Grant Agency of the Czech Republic (Grants No. 203/02/D048 and 203/04/0490 respectively). The authors thank also the Marie Curie Research and Training Network (Grant No. 505 027, POLYAMPHI) for the support. Finally, we thank Dr. R. Hutterer for kind reading of the manuscript and for his inspiring comments.

References and Notes

(1) Tuzar, Z.; Webber, S. E.; Ramireddy, C.; Munk, P. *Polym. Prepr.* (*Am. Chem. Soc., Div. Polym. Chem.*) **1991**, *32*, 525.

(2) For review, see: Hadjichristidis, N.; Pispas, S.; Floudas, G. A. *Block Copolymers*: *Synthetic Strategies, Physical Properties and Applications*; Wiley-Interscience: Hoboken, NJ, 2003; pp 203−231.

(3) (a) Štěpánek, M.; Podhájecká, K.; Tesařová, E.; Procházka, K.; Tuzar, Z.; Brown, W. *Langmuir* **2001**, *17*, 4240. (b) Podhájecká, K.; Štěpánek, M.; Procházka, K.; Brown, W. *Langmuir* **2001**, *17*, 4245.

(4) Erhardt, R.; Böker, A.; Zettl, H.; Kaya, H.; Pychhout-Hintzen, W.; Krausch, G.; Abetz, V.; Müller A. H. E. *Macromolecules* **2001**, *34*, 1069.

(5) (a) Procházka, K.; Martin, T. J.; Webber, S. E.; Munk, P. *Macromolecules* **1996**, *29*, 6526. (b) Talingting, M. R.; Munk, P.; Webber, S. E.; Tuzar, Z. *Macromolecules* **1999**, *32*, 1593.

(6) (a) Štěpánek, M.; Humpolíčková, J.; Procházka, K.; Hof, M.; Tuzar, Z.; Špírková, M.; Wolff, T. *Collect. Czech. Chem. Commun.* **2003**, *68*, 2120. (b) Štěpánek, M.; Matějíček, P.; Humpolíčková, J.; Procházka, K. *Langmuir* **2005**, *21*, 10783.

(7) Light scattering from polyelectrolytes solutions is usually measured at high ionic strength to obtain regular results unaffected by electrostatic interactions. However, in the case of PS−PVP−PEO micelles, electrostatic repulsion between protonized PVP is required to prevent the aggregation. Although the number fraction of aggregates in more concentrated HCl, where electrostatic repulsion is screened by H^+ and Cl^- ions in, is fairly low, their contribution to the overall scattering cannot be neglected.

(8) *Polymer Handbook*, 3rd ed.; Brandup, J., Immergut, E. H., Eds.; Wiley-Interscience: New York, 1989.

(9) Bliznyuk, V. N.; Assender, H. E.; Briggs, G. A. D. *Macromolecules* **2002**, *35*, 6613.

(10) Tsitsilianis, C.; Voulgaris, D.; Štěpánek, M.; Podhájecká, K.; Procházka, K.; Tuzar, Z.; Brown, W. *Langmuir* **2000**, *16*, 6868.

(11) Hof, M. In *Solvent Relaxation in Biomembranes (Applied Fluorescnce in Chemistry, Biology and Medicine)*; Rettig, W., Ed.; Springer-Verlag: Berlin, 1999; p 439.

(12) Hutterer, R.; Schneider, F. W.; Sprinz, H.; Hof, M. *Biophys. Chem.* **1996**, *61*, 151.

(13) Hutterer, R.; Schneider, F. W.; Hermens, W. T.; Wagenvoord, R.; Hof, M. *Biochim. Biophys. Acta* **1998**, *1414*, 155.

(14) Hutterer, R.; Schneider, F. W.; Lanig, H.; Hof, M. *Biochim. Biophys. Acta* **1997**, *1323*, 195.

(15) Hutterer, R.; Schneider, F. W.; Hof, M. *J. Fluoresc.* **1997**, *7*, 27.

(16) Egelhaaf, H.-J.; Lehr, M.; Hof, M.; Häfner, A.; Fritz, H.; Schneider, F. W.; Bayer, E.; Oelkrug, D. *J. Fluoresc.* **2000**, *10*, 383.

(17) (a) Frauchiger, L.; Shirota, H.; Uhrich, K. E.; Castner, E. W., Jr. *J. Phys. Chem. B* **2002**, *106*, 7463. (b) Shirota, H.; Segawa, H. *J. Phys. Chem. A* **2003**, *107*, 3719. (c) Tamoto, Y.; Segawa, H.; Shirota, H. *Langmuir* **2005**, *21*, 3757.

(18) (a) Chakrabarty, D.; Hazra, P.; Chakraborty, A.; Sarkar, N. *J. Phys. Chem. B* **2003**, *107*, 13643. (b) Chakrabarty, D.; Hazra, P.; Chakraborty, A.; Sarkar, N. *Chem. Phys. Lett.* **2003**, *382*, 71. (c) Hazra, P.; Chakrabarty, D.; Chakraborty A.; Sarkar, N. *Chem. Phys. Lett.* **2004**, *392*, 340. (d) Chakrabarty, D.; Chakraborty A.; Seth, D.; Hazra, P.; Sarkar, N. *J. Chem. Phys.* **2005**, *122*, Art. No. 184516. (e) Bhattachryya, K. *Acc. Chem. Res.* **2003**, *36*, 95.

(19) Horng, M. L.; Gardecki, J. A.; Papazyan, A.; Maroncelli, M. *J. Phys. Chem.* **1995**, *99*, 17311.

(20) Jimenez, R.; Fleming, G. R.; Kumar, P. V.; Maroncelli, M. *Nature* **1994**, *369*, 471.

(21) Sýkora, J.; Kapusta, P.; Fidler, V.; Hof, M. *Langmuir* **2002**, *18*, 571.

(22) (a) Matějíček, P.; Podhájecká, K.; Humpolíčková, J.; Uhlík, F.; Jelínek, K.; Limpouchová, Z.; Procházka, K.; Špirková, M. *Macromolecules* **2004**, *37*, 10141. (b) Uhlík, F.; Limpouchová, Z.; Jelínek, K.; Procházka, K. *J. Chem. Phys.* **2004**, *121*, 2367.

(23) Hutterer, R.; Parusel, A. B. J.; Hof, M. *J. Fluoresc.* **1998**, *8*, 389.

(24) Hutterer, R.; Hof, M. *J. Fluoresc.* **2001**, *11*, 227.

(25) Hutterer, R.; Hof, M. *Z. Phys. Chem.* **2002**, *216*, 1.

(26) Sýkora, J.; Mudogo, V.; Hutterer, R.; Nepraš, M.; Vanìrka, J.; Kapusta, P.; Fidler, V.; Hof, M. *Langmuir* **2002**, *18*, 9276.

(27) Fee, R. S.; Maroncelli, M. *Chem. Phys.* **1994**, *183*, 235.

(28) Yang, M.; Richert, R. *J. Chem. Phys.* **2001**, *115*, 2676.

(29) Richert, R. *J. Phys. Chem.* **2001**, *115*, 1429.

(30) Stubbs, C. D.; Williams, B. W. In *Topics in Fluorescence Spectroscopy*: *Biochemical Applications*; Lakowicz, J. R., Ed.; Plenum Press: New York, 1992; p 231.

(31) Martin, T. J.; Procházka, K.; Munk, P.; Webber, S. E. *Macromolecules* **1996**, *29*, 6071.

(32) Hertz, H. G. *Water, A Comprehensive Treatise*; Plenum Press: New York, 1973; Vol. 3, Chapter 7.

(33) Bieze, T. W. N.; Barnes, A. C.; Huige, C. J. M.; Enderby, J. E.; Leyte, J. C. *J. Phys. Chem.* **1994**, *98*, 6568.

(34) Blandamer, M. J.; Fox, M. F.; Powell, E.; Stafford, J. W. *Makromol. Chem.* **1967**, *124*, 222.

(35) Toryanik, A. I. *Zh. Struct. Khim.* **1984**, *25*, 49.

(36) *Hydrogen-Bonded Liquids*; Bellisent-Funel, M. C., Ed.; NATO ASI Series, Series C; Kluwer Academic: Dordrecht, 1989; Chapter III(3).

(37) Soper, A.; Phillips, M. S. *J. Phys. Chem.* **1988**, *92*, 47.